



Title	Theoretical study on elastic properties of $\text{Si}_2\text{N}_2\text{O}$ by ab initio calculation
Author(s)	Tsuboi, Seiya; Adachi, Kanta; Nagakubo, Akira et al.
Citation	Japanese Journal of Applied Physics. 2018, 57, p. 07LB04
Version Type	AM
URL	https://hdl.handle.net/11094/84173
rights	
Note	

The University of Osaka Institutional Knowledge Archive : OUKA

<https://ir.library.osaka-u.ac.jp/>

The University of Osaka

Theoretical study on elastic properties of $\text{Si}_2\text{N}_2\text{O}$ by ab initio calculation

Seiya Tsuboi¹, Kanta Adachi¹, Akira Nagakubo,² and Hirotsugu Ogi^{3*}

¹Graduate School of Engineering Science, Osaka University, Toyonaka, Osaka 560-8531, Japan

²Institute for Chemical Research, Kyoto University, Uji, Kyoto 611-0011, Japan

³Graduate School of Engineering, Osaka University, Suita, Osaka 565-0871, Japan

The elastic constants of crystalline $\text{Si}_2\text{N}_2\text{O}$ remain unknown since it was discovered in 1960s. We determine the nine independent elastic constants of orthorhombic $\text{Si}_2\text{N}_2\text{O}$ by *ab-initio* calculations. We applied various deformation modes with strains up to ± 0.01 to the unit cell, calculated the energy-strain relationships, and deduced all the elastic constants by fitting the harmonic-oscillation function. Our results are as follows: $C_{11}=311.1$, $C_{22}=238.5$, $C_{33}=317.9$, $C_{44}=136.1$, $C_{55}=57.6$, $C_{66}=73.9$, $C_{12}=79.6$, $C_{13}=52.2$, and $C_{23}=33.6$ GPa. Despite different crystal structures and symmetries, the direction-over-averaged Young's modulus of $\text{Si}_2\text{N}_2\text{O}$ is well explained by the nitrogen content and Young's moduli of $\alpha\text{-SiO}_2$ and $\beta\text{-Si}_3\text{N}_4$. Anisotropy of sound-wave velocity was investigated, and its origin was discussed by the crystallographic structure. The quasi-isotropic plane for the longitudinal-wave propagation was identified.

1. Introduction

The word *silicon oxynitride* normally indicates non-crystalline silicon-nitrogen-oxygen compounds in the field of electronics devices. It exhibits amorphous structure with various nitrogen compositions between amorphous SiO_2 and amorphous Si_3N_4 . The amorphous silicon oxynitride has been attracted as optical elements because its refractive index also changes between SiO_2 and Si_3N_4 in response to its composition.¹⁻⁴⁾ On the other hand, silicon oxynitride occasionally represents crystalline silicon-nitrogen-oxygen compounds with chemical formula of $\text{Si}_2\text{N}_2\text{O}$. It was discovered in 1960s⁵⁾ and is the only stable crystalline compound between SiO_2 and Si_3N_4 .

The crystalline $\text{Si}_2\text{N}_2\text{O}$ can be synthesized by heating silicon and quartz powder in nitrogen atmosphere at $1,450^\circ\text{C}$.⁵⁾ It is an important high-temperature material because of its promising heat characteristics: It exhibits high flexural strength up to $1,300^\circ\text{C}$ in addition to strong resistance to oxidation and thermal shock.⁶⁾ On the other hand, elastic properties of $\text{Si}_2\text{N}_2\text{O}$ have not been studied in detail. It is well recognized that amorphous SiO_2 shows the positive temperature coefficient of velocity (TCV) near room temperature,⁷⁾ which is the opposite trend to usual materials, and used for temperature compensation in acoustic resonator devices.⁸⁻¹³⁾ On the other hand, Si_3N_4 shows ordinary (negative) TCV.¹⁴⁾ The crystalline $\text{Si}_2\text{N}_2\text{O}$ could be then a promising material for acoustic resonators because its TCV is expected to be very small. Therefore, it is highly important to elucidate its elastic constants and sound propagation behavior. However, there is no report on experimental nor theoretical

*E-mail: ogi@prec.eng.osaka-u.ac.jp

study of the elastic constants of the crystalline $\text{Si}_2\text{N}_2\text{O}$.

Here, we determine all of the independent elastic constants of $\text{Si}_2\text{N}_2\text{O}$ using *ab-initio* calculations along with those of $\alpha\text{-SiO}_2$ and $\beta\text{-Si}_3\text{N}_4$ for comparison and investigate the sound propagation behavior in various directions.

2. Calculation Method

2.1 Materials

$\text{Si}_2\text{N}_2\text{O}$ belongs to the space group $Cmc2_1$,⁵⁾ showing orthorhombic symmetry. It then exhibits nine independent elastic constants:

$$C_{ij} = \begin{pmatrix} C_{11} & C_{12} & C_{13} & 0 & 0 & 0 \\ C_{12} & C_{22} & C_{23} & 0 & 0 & 0 \\ C_{13} & C_{23} & C_{33} & 0 & 0 & 0 \\ 0 & 0 & 0 & C_{44} & 0 & 0 \\ 0 & 0 & 0 & 0 & C_{55} & 0 \\ 0 & 0 & 0 & 0 & 0 & C_{66} \end{pmatrix} \quad (1)$$

As shown in Fig. 1(a), $\text{Si}_2\text{N}_2\text{O}$ consists of Si centered $[\text{SiN}_3\text{O}]$ tetrahedrons connecting with each other via shared vertices.¹⁵⁾

Crystalline $\alpha\text{-SiO}_2$ is composed of $[\text{SiO}_4]$ tetrahedrons. As shown in Fig. 1(b), its symmetry and space group are trigonal and $P3_121$, respectively, showing six independent elastic constants (C_{11} , C_{12} , C_{13} , C_{14} , C_{33} , and C_{44}).

Si_3N_4 takes two principal types of crystal structures ($\alpha\text{-Si}_3\text{N}_4$ or $\beta\text{-Si}_3\text{N}_4$). We chose $\beta\text{-Si}_3\text{N}_4$ as the calculation target because of its stability at a temperature range, including room temperature. It shows hexagonal symmetry with five independent elastic constants (C_{11} , C_{12} , C_{13} , C_{33} , and C_{44}). Space group of $\beta\text{-Si}_3\text{N}_4$ is controversial and possibly be $P6_3/m$ or $P6_3$.¹⁶⁾ We performed the calculation using $P6_3$, which allows successful calculation results as will be shown.

We performed calculations of lattice parameters and the elastic constants of the three types of Si-O-N compounds, which have similar structures in terms of being made of tetrahedron centering around Si atoms.

2.2 Calculation details

We used the *Vienna Ab-initio* Simulation Package (VASP),¹⁷⁾ which calculates total energy based on the density functional theory. The VASP works as if it calculated all electrons, including core electrons, due to the projector-augmented-wave (PAW) method. For the exchange correlation potential, we employed the local-density-approximation (LDA)¹⁸⁾ and generalized-gradient-approximation (GGA)¹⁹⁾ methods. We set k -point meshes and the energy cutoff to be $10 \times 10 \times 10$ and 1,000 eV, respectively. The computation was carried out using the computer facilities at Research Institute of Information Technology, Kyushu University.

First, we determined the lattice constants and atomic sites at the ground state by minimizing the

total energy and the internal stresses, varying the cell volume, shape, and atomic positions.

Next, the elastic constants C_{ij} were determined by applying various deformations to the unit cell, calculating changes in the total energy, and fitting the harmonic function to the relationships between the energy and the strain. We applied the representative strain up to ± 0.01 in each deformation mode, where the system was relaxed at individual strain state and the energy was determined.^{20–23)} The total energy can be written as follows, ignoring the higher order terms:²⁴⁾

$$E(V, S) = E(V_0, 0) + V_0 \left(\sum_I \tau_I S_I + \frac{1}{2} \sum_{I,J} C_{IJ} S_I S_J \right). \quad (2)$$

Here, V , V_0 , τ and S denote the cell volume, that at the ground state, residual stress, and the engineering strain, respectively. The elastic constants are then deduced by fitting the quadratic function to Eq. (2).

3. Results and discussions

The lattice constants determined in this study are compared with experiments in Table I.¹⁵⁾ Differences between our calculations and reported experimental values are less than 0.32%, 0.63%, and 0.55% for $\text{Si}_2\text{N}_2\text{O}$, $\alpha\text{-SiO}_2$, and $\beta\text{-Si}_3\text{N}_4$, respectively, in case of LDA potentials. As to GGA, they are up to 1.4%, 2.524%, and 0.90% for $\text{Si}_2\text{N}_2\text{O}$, $\alpha\text{-SiO}_2$, and $\beta\text{-Si}_3\text{N}_4$, respectively. It is, therefore, notable that LDA potentials are more proper for theoretically calculating properties of these Si-O-N compounds, and we determined the elastic constants using LDA exchange correlation potentials.

Figure 2 shows examples of the relationships between the total energy and the applied strain for $\text{Si}_2\text{N}_2\text{O}$ together with the fitted solid curves, which indicates significant anisotropy between C_{22} and C_{33} , and between C_{44} and C_{55} : The energy increase becomes larger by applying $S_4(=2\epsilon_{23})$ than $S_5(=2\epsilon_{13})$, for example. Favorable fitting results confirm the reliability of the determined values. Our values and reported experimental values are compared in Table II. Concerning $\beta\text{-Si}_3\text{N}_4$, our calculations agree with measurements within 10%, even for the off-diagonal components, which are usually less accurately determined because of weak contribution to deformation. As for $\alpha\text{-SiO}_2$, our calculations are favorably compared with measurements except for C_{14} . The discrepancy in C_{14} may be acceptable, because both in calculation and experiment, C_{14} is inherently inaccurately determined because of its very low sensitivity to deformation. Because of higher symmetry of $\text{Si}_2\text{N}_2\text{O}$ ($C_{14}=0$) than $\alpha\text{-SiO}_2$, we expect that the C_{ij} of $\text{Si}_2\text{N}_2\text{O}$ are determined within $\sim 10\%$ error.

Using the obtained C_{ij} values, we calculated the Young moduli E_i and the Poisson ratios ν_{ij} in the principal directions, and the Bulk modulus B (Table III). It is not straightforward to compare these values among the different-symmetry crystals. We then computed the direction-over-averaged elastic constants (isotropic C_{11} and C_{12} , Young modulus E^{ave} , and Bulk modulus B^{ave} .) using the Hill approximation method,^{29–31)} which are also given in Table III. Surprisingly, the averaged elastic constants of $\text{Si}_2\text{N}_2\text{O}$ are accurately estimated by those of $\alpha\text{-SiO}_2$ and $\beta\text{-Si}_3\text{N}_4$, and the nitrogen content, despite their different crystallographic symmetry. For example, Figure 3 shows such a relationship for E^{ave} , where the averaged Young moduli of the three crystals are connected by a straight line with the

correlation coefficient of 0.9991.¹⁵⁾ This is a very important finding because many other properties (mechanical, electric, ...) of $\text{Si}_2\text{N}_2\text{O}$ could be accurately estimated from those of $\alpha\text{-SiO}_2$ and $\beta\text{-Si}_3\text{N}_4$.

Next, we discuss the sound-velocity anisotropy in $\text{Si}_2\text{N}_2\text{O}$. We calculated velocities of ultrasound propagating in various directions by solving the Christoffel equation using obtained C_{ij} and mass density $\rho = 2826 \text{ kg/m}^3$. Figure 4 shows propagation behaviors in the three orthogonal planes and corresponding projection crystal structures. The longitudinal-wave velocity in the Y axis is smaller than those in X and Z axes (Fig. 4(a) and (b)) because of significantly smaller C_{22} . This can be explained by the bending of the tetrahedron at the nitrogen vertex: $\text{Si}_2\text{N}_2\text{O}$ consists of the network structure of silicon-centered tetrahedrons, sharing nitrogen and oxygen vertexes. Each tetrahedron is stable and will be rigid-like unit. Thus, the bending at the vertex will dominate crystal's deformation. Structures in Figs. 4(a) and (b) indicate that the longitudinal loading along the Y axis will induce the network bending at the nitrogen vertexes, leading to slow velocity. The velocity anisotropy becomes more significant for shear waves. Figure 4 shows shear-wave propagation behaviors on the orthogonal planes; blue lines denote in-plane and out-of-plane polarized shear waves. Shear waves polarized in the YZ plane show markedly larger velocities, and this trend is caused by significantly larger C_{44} than C_{55} and C_{66} . This anisotropy for shear deformation is also attributed to the bending of the tetrahedron at the shearing vertex. The crystal structure in the YZ plane (Fig. 4(b)) suggests high rigidity to the shear deformation in the YZ plane. On the other hand, the projection structures in XY (Fig. 4(a)) and ZX (Fig. 4(c)) planes indicate that the shear deformation in these planes will be easily caused by the bending of the tetrahedron network at the oxygen vertexes.

Finally, we propose a specific plane (9 0 20), on which longitudinal waves travel with nearly the same velocity, as if the crystal were isotropic (Fig. 5). This characteristic will be useful in designing acoustic devices such as resonators.

4. Conclusion

We determined the complete set of elastic constants of $\text{Si}_2\text{N}_2\text{O}$ by *ab-initio* calculations, where it is revealed that LDA exchange correlation potentials are more suitable. The direction-over-averaged elastic constants are surprisingly accurately estimated by those of $\alpha\text{-SiO}_2$ and $\beta\text{-Si}_3\text{N}_4$, and the nitrogen content. In particular, averaged Young's modulus nearly lays on the line connecting those of $\alpha\text{-SiO}_2$ and $\beta\text{-Si}_3\text{N}_4$. Thus, any properties of $\text{Si}_2\text{N}_2\text{O}$ are expected to be estimated by corresponding properties of $\alpha\text{-SiO}_2$ and $\beta\text{-Si}_3\text{N}_4$, and the nitrogen content. The sound-wave anisotropy was investigated, and its origin was explained in the crystallographic view by the bending behavior of the Si-centered tetrahedron network at the nitrogen and oxygen vertexes. Furthermore, we find a specific plane (9 0 20), on which the longitudinal wave propagates without direction anisotropy.

References

- 1) B. Tryggve: Appl. Opt. **21** (1982) 1069.
- 2) J. Viard, E. Beche, D. Perarnau, R. Berjoan, and J. Durand: J. Europ. Ceram. Soc. **17** (1997) 2025.
- 3) J. R. Shallenberger, D. A. Cole, and S. W. Novak: J. Vac. Sci. Technol. A **17** (1999) 1086.
- 4) F. Rebib, E. Tomasella, E Bêche, J. Cellier, and M. Jacquet: J. Phys.: Conf. Ser. **100** (2008) 082034.
- 5) C. Brosset and I. Idrestedt: Nature **201** (1964) 1211.
- 6) M. Ohashi, H. Tabata and S. Kanzaki: J. Mater. Sci. Lett. **7** (1988) 339.
- 7) R. Vacher, J. Pelous, F. Plicque, and A. Zarembowitch: J. Non-Crystalline Solids **45** (1981) 397.
- 8) J. W. Marx and J. M. Sivertsen: J. Appl. Phys. **24** (1953) 81.
- 9) S. Spinner: J. Am. Ceram. Soc. **39** (1956) 113.
- 10) T. E. Parker and H. Wichansky: J. Appl. Phys. **50** (1979) 1360.
- 11) H. Nakanishi, H. Nakamura, T. Tsurunari, J. Fujiwara, Y. Hamaoka, and K. Hashimoto: Jpn. J. Appl. Phys. **50** (2011) 07HD13.
- 12) A. Nagakubo, H. Ogi, H. Ishida, M. Hirao, T. Yokoyama, and T. Nishihara: J. Appl. Phys. **118** (2015) 014307.
- 13) G. Tang, T. Han, A. Teshigahara, T. Iwaki, and K. Hashimoto: Jpn. J. Appl. Phys. **55** (2016) 07KD07.
- 14) K.J. Singh, Y. Matsuda, K. Hattori, H. Nakano, and S. Nagai: Ultrasonics **41** (2003) 9.
- 15) S. Tsuboi, K. Adachi, A. Nagakubo, and H. Ogi: Proc. Symp. Ultrason. Electron. **38** (2017) 1P1-6.
- 16) R. Belkada, M. Kohyama, T. Shibayanagi and M. Naka: Phys. Rev. B **65** (2002) 092104.
- 17) G. Kresse and J. Hafner: Phys. Rev. B **47** (1993) 558.
- 18) D. M. Ceperley and B. J. Alder: Phys. Rev. Lett. **45** (1980) 566 .
- 19) J. P. Perdew, K. Burke and M. Ernzerhof: Phys. Rev. Lett. **77** (1996) 3865.
- 20) H. Tanei, K. Tanigaki, K. Kusakabe, H. Ogi, N. Nakamura, and M. Hirao: Appl. Phys. Lett. **94** (2009) 041914.
- 21) A. Nagakubo, H. Ogi, H. Sumiya, K. Kusakabe, and M. Hirao: Appl. Phys. Lett. **102** (2013) 241909.
- 22) K. Tanigaki, H. Ogi, H. Sumiya, K. Kusakabe, N. Nakamura, M. Hirao, and H. Ledbetter: Nat. Commun. **4** (2013) 2343.
- 23) K. Adachi, H. Ogi, A. Nagakubo, N. Nakamura, M. Hirao, M. Imade, M. Yoshimura, and Y. Mori: J. Appl. Phys. **119** (2016) 245111.
- 24) L. Fast, J. M. Wills, B. Johansson, and O. Eriksson: Phys. Rev. B **51** (1995) 17431.

- 25) Y. Xu and W. Y. Ching: Phys. Rev. B **51** (1995) 24.
- 26) R. Grün: Acta Crystallogr., Sect. B **35** (1979) 800.
- 27) R. Tarumi, K. Nakamura, H. Ogi and M. Hirao: J. Appl. Phys. **102** (2007) 113408.
- 28) R. Vogelgesang and M. Grimsditch: Appl. Phys. Lett. **76**, (2000) 982.
- 29) R. Hill: Proc. Phys. Soc. A **65** (1952) 349.
- 30) H. Ledbetter, H. Ogi, S. Kai, S. Kim, and M. Hirao: J. Appl. Phys. **95** (2004) 4642 (2004).
- 31) H. Ogi, N. Nakamura, H. Tanei, R. Ikeda, M. Hirao, and Mikio Takemoto: Appl. Phys. Lett. **86** (2005) 231904.

Table I. Lattice constants obtained by the relaxation calculation and reported values (in units of Å).

		<i>a</i>	<i>b</i>	<i>c</i>
Si ₂ N ₂ O	LDA	8.871	5.489	4.838
	GGA	8.967	5.550	4.898
	Experimental ⁵⁾	8.843	5.473	4.835
α -SiO ₂	LDA	4.882	$a = b$	5.381
	GGA	5.037	$a = b$	5.525
	Experimental ²⁵⁾	4.913	$a = b$	5.405
β -Si ₃ N ₄	LDA	7.578	$a = b$	2.893
	GGA	7.663	$a = b$	2.926
	Experimental ²⁶⁾	7.595	$a = b$	2.902

Table II. Elastic constants calculated with LDA potentials and those reported (in units of GPa).

	$\text{Si}_2\text{N}_2\text{O}$		$\alpha\text{-SiO}_2$	$\beta\text{-Si}_3\text{N}_4$	
	this work	this work	Experimental ²⁷⁾	this work	Experimental ²⁸⁾
C_{11}	311.1	72.9	86.76	422.9	433
C_{22}	238.5	-	-	-	-
C_{33}	317.9	96.6	105.41	553.9	574
C_{44}	136.1	52.2	58.27	99.1	108
C_{55}	57.6	-	-	-	-
C_{66}	73.9	-	-	-	-
C_{12}	79.6	7.6	7.06	199.3	195
C_{13}	52.2	7.8	11.90	117.7	127
C_{23}	33.6	-	-	-	-
C_{14}	-	-0.1	-17.98	-	-

Table III. Young modulus E_i [GPa], Bulk modulus B [GPa], Poisson ratio ν_{ij} , direction-averaged elastic constants $C_{ij}^{ave.}$ [GPa], averaged Young modulus $E^{ave.}$ [GPa] and averaged Bulk modulus $B^{ave.}$ [GPa]

	Si ₂ N ₂ O	α -SiO ₂	β -Si ₃ N ₄
E_1	279.4	71.5	321.5
E_2	216.8	E_1	E_1
E_3	307.3	95.1	509.3
B	130.7	31.6	251.7
ν_{12}	0.3152	0.0970	0.4380
ν_{13}	0.1307	0.0730	0.1195
ν_{21}	0.2447	ν_{12}	ν_{12}
ν_{23}	0.0656	ν_{13}	ν_{13}
ν_{31}	0.1439	0.0971	0.1892
ν_{32}	0.0930	ν_{31}	ν_{31}
$C_{11}^{ave.}$	258.3	86.5	413.9
$C_{12}^{ave.}$	68.8	4.5	170.9
$E^{ave.}$	229.4	86.1	314.0
$B^{ave.}$	131.9	31.8	251.9

Figure Captions

Fig. 1. (Color online) The crystal structures of (a) $\text{Si}_2\text{N}_2\text{O}$, (b) $\alpha\text{-SiO}_2$ and (c) $\beta\text{-Si}_3\text{N}_4$. The blue, silver and red balls represent silicon, nitrogen and oxygen atoms, respectively.

Fig. 2. Relationships between the total energy and applied strain when (a) ϵ_{33} and ϵ_{22} are applied and when (b) ϵ_{23} and ϵ_{13} are applied.

Fig. 3. Relationship between nitrogen atom content and the averaged Young modulus.

Fig. 4. (Color online) Sound-velocity mappings (left) in (a) XY-, (b) YZ-, and (c) ZX-planes, and corresponding crystal structures (right). Red and blue lines represent the longitudinal and shear waves. Blue tetrahedron represents the Si-centered tetrahedron, and red and silver balls denote oxygen and nitrogen atoms, respectively.

Fig. 5. (Color online) Directional dependence of sound velocities propagating along (9 0 20) plane. Red and blue lines represent longitudinal and shear waves.

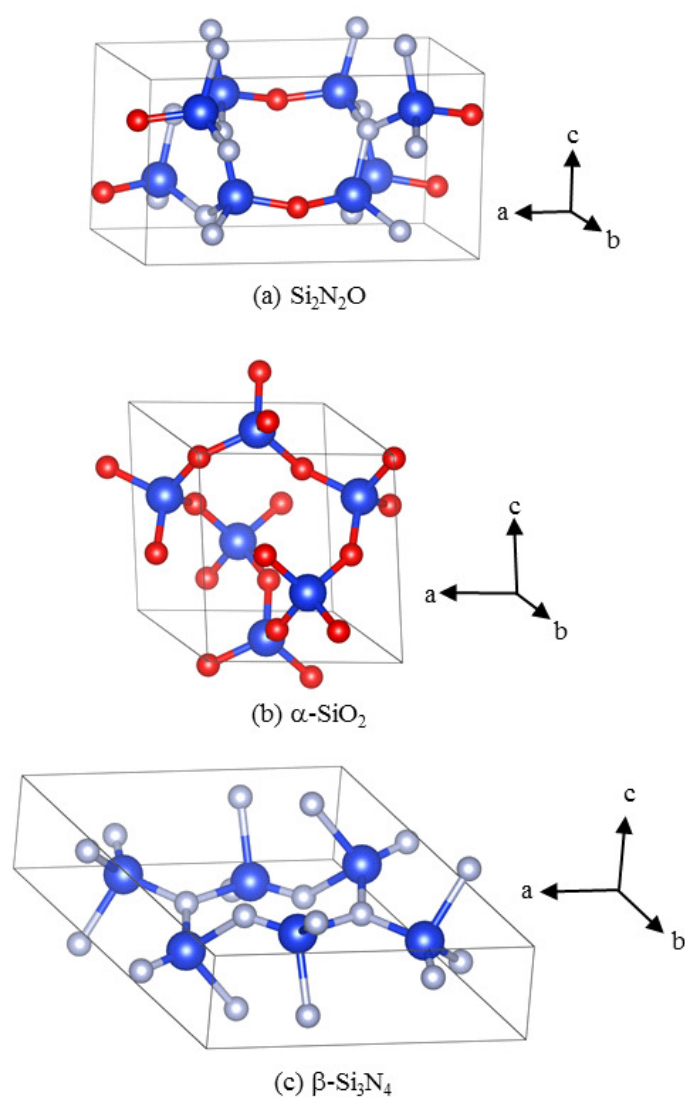


Fig. 1.

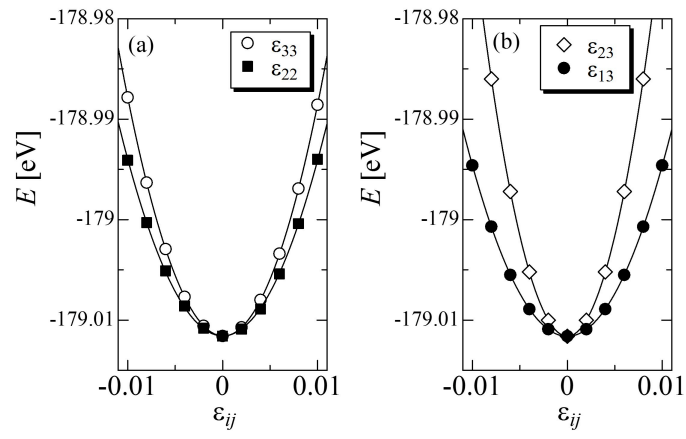


Fig. 2.

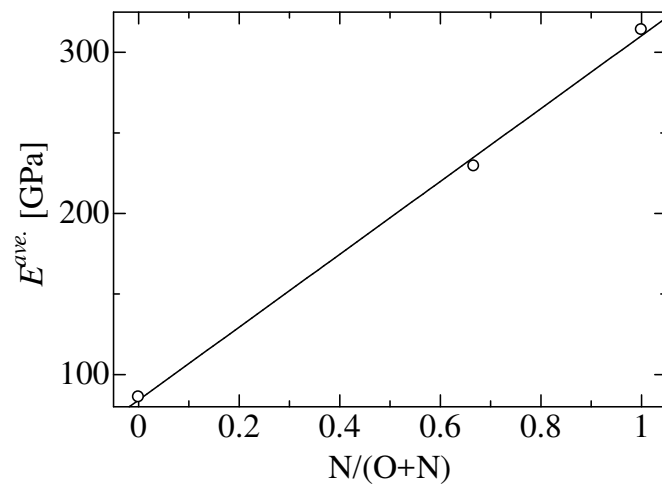


Fig. 3.

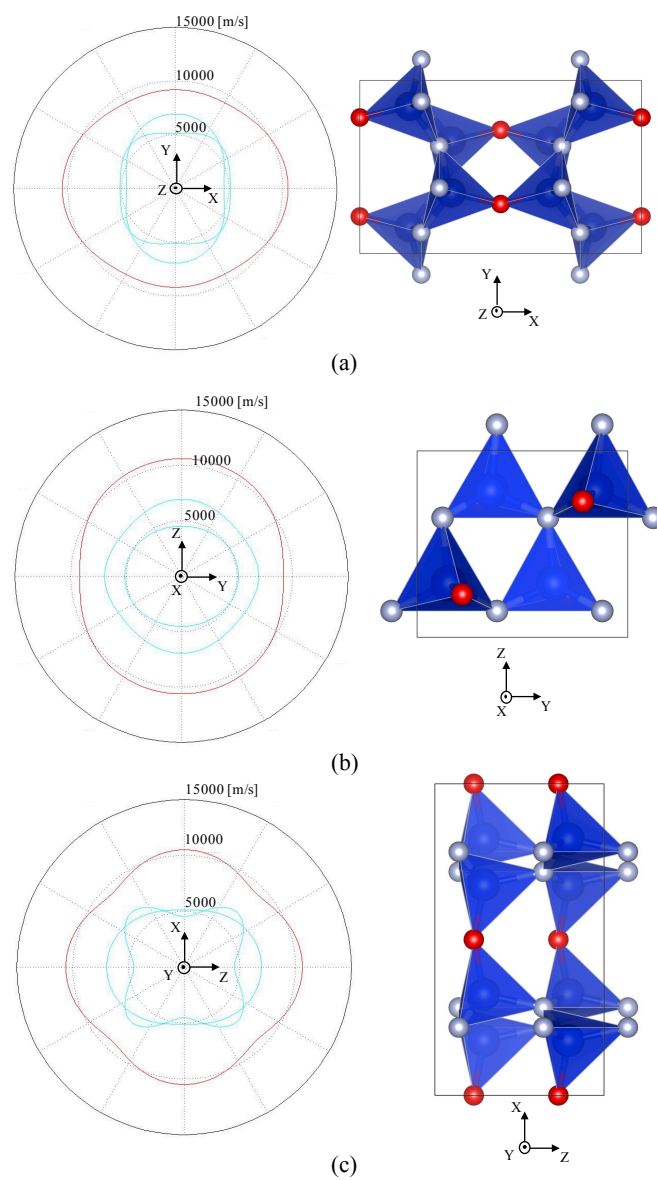


Fig. 4.

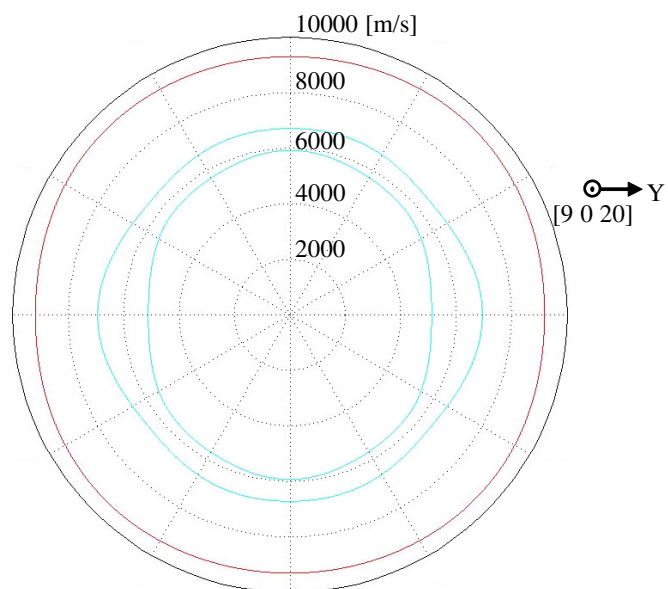


Fig. 5.